

Versatility of a localized surface plasmon resonance-based gold nanoparticle-alloyed quantum dot nanobiosensor for immunofluorescence detection of viruses

メタデータ	言語: eng 出版者: 公開日: 2018-09-13 キーワード (Ja): キーワード (En): 作成者: Takemura, Kenshin, Adegoke, Oluwasesan, Takahashi, Naoto, Kato, Tatsuya, Li, Tian-Cheng, Kitamoto, Noritoshi, Tanaka, Tomoyuki, Suzuki, Tetsuro, Park, Enoch Y. メールアドレス: 所属:
URL	http://hdl.handle.net/10297/00025706

Versatility of a localized surface plasmon resonance-based gold nanoparticle-alloyed quantum dot nanobiosensor for immunofluorescence detection of viruses

Kenshin Takemura^a, Oluwasesan Adegoke^b, Naoto Takahashi^a, Tatsuya Kato^{b,c}, Tian-Cheng Li^d, Noritoshi Kitamoto^e, Tomoyuki Tanaka^f, Tetsuro Suzuki^g, and Enoch Y. Park^{b,c,*}

^a *Laboratory of Biotechnology, Department of Agriculture, Graduate School of Integrated Science and Technology, Shizuoka University, 836 Ohya, Suruga-ku, Shizuoka 422-8529, Japan*

^b *Laboratory of Biotechnology, Research Institute of Green Science and Technology, Shizuoka University, 836 Ohya, Suruga-ku, Shizuoka 422-8529, Japan*

^c *College of Agriculture, Academic Institute, Shizuoka University, 836 Ohya, Suruga-ku, Shizuoka 422-8529, Japan*

^d *Department of Virology II, National Institute of Infectious Diseases, Gakuen 4-7-1, Musashi-Murayama, Tokyo 208-0011, Japan*

^e *School of Human Science and Environment, University of Hyogo, 1-1-12 Shinzaike-Honcho, Himeji, Hyogo 670-0092, Japan*

^f *Hidaka General Hospital, Gobo, Wakayama 644-0002, Japan*

^g *Department of Infectious Diseases, Hamamatsu University School of Medicine, 1-20-1 Higashi-ku, Handa-yama, Hamamatsu 431-3192, Japan*

E-mail:

kenpi901@yahoo.co.jp (KT)

adegoke.sesan@mailbox.co.za (OA)

pakkun0449@yahoo.co.jp (TN)

kato.tatsuya@shizuoka.ac.jp (TK)

litc@nih.go.jp (TCL)

kitamoto@shse.u-hyogo.ac.jp (NK)

moqui-tom@maia.eonet.ne.jp (TT)

tesuzuki@hama-med.ac.jp (TS)

park.enoch@shizuoka.ac.jp (EYP)

* Correspondence to: Research Institute of Green Science and Technology, Shizuoka University, 836 Ohya Suruga-ku, Shizuoka, 422-8529, Japan. Tel. & fax: +81 54 238 4887. E-mail address: park.enoch@shizuoka.ac.jp (EYP)

Abstract

Flu infection, caused by the influenza virus, constitutes a serious threat to human lives worldwide. A rapid, sensitive and specific diagnosis is urgently needed for point-of-care treatment and to control the rapid spread of this disease. In this study, an ultrasensitive, rapid and specific localized surface plasmon resonance (LSPR)-induced immunofluorescence nanobiosensor has been developed for the influenza virus based on a gold nanoparticle (AuNP)-induced quantum dot (QD) fluorescence signal. Alloyed quaternary CdSeTeS QDs were synthesized via the hot-injection organometallic route and were subsequently capped with L-cysteine via a ligand exchange reaction. AuNPs were synthesized in HEPES buffer and thiolated with L-cysteine. The concept of the biosensor involves the conjugation of anti-neuraminidase (NA) antibody (anti-NA Ab) to thiolated AuNPs and the conjugation of anti-hemagglutinin (HA) antibody (anti-HA Ab) to alloyed quaternary L-cysteine-capped CdSeTeS QDs. Interaction of the antigens displaying on the surface of the influenza virus target with anti-NA Ab-conjugated AuNPs and anti-HA Ab-conjugated QDs induces an LSPR signal from adjacent AuNPs to trigger fluorescence-enhancement changes in the QDs in proportion to the concentration of the target virus. The detection limit for influenza H1N1 virus was 0.03 pg/mL in deionized water and 0.4 pg/mL in human serum; while, for the clinically isolated H3N2, the detection limit was 10 PFU/mL. The detection of influenza virus H1N1 was accomplished with high sensitivity. The versatility of the biosensor was demonstrated for the detection of clinically isolated influenza virus H3N2 and norovirus-like particles (NoV-LPs).

KEYWORDS: Localized surface plasmon resonance, Gold nanoparticle, Alloyed quantum dot, Immunofluorescence detection, Influenza virus, Norovirus

1. Introduction

Influenza viruses are classified into three genera types, namely influenza virus A, B and C. Among them, influenza virus A is the most common because it carries the infectious human pathogen and because it is highly diversified and easily mutated (**Christman et al., 2011; Hay et al., 2001; Leung et al., 2014**). The pandemic influenza virus A H1N1 that occurred in 2009 caused an outbreak of respiratory infection that emanated from Mexico and spread globally to 191 countries (**Girarda et al., 2010; Özyer et al., 2011**). This outbreak induced a worldwide challenge for health experts and researchers, with the primary aim of developing efficient ways to prevent the rapid spread of this disease (**Bimbo et al., 2013; Grabowska et al., 2013**).

Conventional diagnostic systems used for the influenza virus have certain limitations that have inspired the continuous development of efficient probes that are capable of meeting the demand for high sensitivity, selectivity and rapidity. Antibody (Ab) detection of the virus based on serological analysis can lead to vague and misguided data interpretation (**Centers for Disease Control and Prevention**). The commercial rapid influenza detection test (RIDTS) is prone to false-positive and false-negative results (**Landry, 2011**). Viral culture analysis is time consuming (**Treanor et al., 2005**), while existing immunofluorescence assays are cheap but limited in their sensitivity (**Lee et al., 2015; Pianciola et al., 2010**). Hence, there is a continued demand for the development of rapid, highly sensitive and selective diagnostic probes for the influenza virus.

Fluorescent semiconductor quantum dot (QD) nanocrystals have been widely used as fluorescence reporters in various biosensor designs (**Ahmed et al., 2014; Lee et al., 2015; Tian et al., 2012**) due to their unique optical properties such as their broad absorption and narrow emission spectra, multiplex detection capabilities, size-tunable emission

spectra, biocompatibility potential and high photostability (**Anderson et al., 2008; Bruchez et al., 1998; Chan et al., 1998**). Recent developments on the applications of QDs in biosensor design have shown that alloyed QD nanocrystals generate higher output efficiencies than conventional binary QD systems (**Adegoke et al., 2016; Adegoke et al., 2016**). It is therefore reasonable to believe that the combination of a metallic nanoparticle with surface plasmon properties could be used to enhance the fluorescence of adjacent QD fluorophores to improve bio-detection sensitivity.

Surface plasmon resonance (SPR) biosensors have been widely used in the fields of biotechnology, biochemistry and bioengineering as diagnostic probes for infectious diseases, ion sensing, protein-DNA interactions, binding events and biological surface modifications (**Campbell et al., 2007; Eum et al., 2003; Jeong et al., 2008; Lee et al., 2015; Patskovsky et al., 2008; Yeom et al., 2013**). Moreover, localized surface plasmon resonance (LSPR) biosensor systems adapted from SPR have drawn active interest in the research community.

In this paper, we report on the rapid and ultrasensitive detection of influenza virus H1N1 using an immunofluorescence biosensor based on a combination of LSPR-induced optical transduction from AuNP-labeled anti-NA Ab and the fluorescence signal generated from adjacent alloyed CdSeTeS QD-labeled anti-HA Ab. The mechanism of the biosensor involves an antigen-antibody interaction in which LSPR induced from AuNPs is used to enhance the fluorescence of adjacent alloyed QDs for the bio-detection of influenza virus. The immunofluorescence biosensor developed in this work is rapid, ultrasensitive and specific. Further analyses demonstrated that the immunofluorescence biosensor developed in this work is also applicable to influenza virus H3N2 and norovirus-like particles (NoV-LPs).

2. Materials and methods

2.1. Materials

HEPES buffer, PBS buffer, polyoxyethylene (20) sorbitan monolaurate (Tween 20), sodium acetate, hydrogen peroxide, sulfuric acid, methanol, potassium hydroxide (KOH), chloroform and acetone were purchased from Wako Pure Chemical Ind. Ltd. (Osaka, Japan). HAuCl_4 , N-(3-dimethylaminopropyl)-N'-ethylcarbodiimide hydrochloride (EDC), N-hydroxysuccinimide (NHS), bovine serum albumin (BSA), 1-octadecene, cadmium oxide (CdO), tellurium (Te), L-cysteine, hexadecylamine (HDA), trioctylphosphine oxide (TOPO), trioctylphosphine (TOP), selenium (Se) and sulfur (S) were purchased from Sigma Aldrich Co., LLC (Saint Louis, MO, USA). Oleic acid was purchased from Nacalai Tesque Inc. (Kyoto, Japan). Anti-NA Ab against influenza A virus NA (N1) (New Caledonia/20/1999) (H1N1) and a rabbit polyclonal Ab were purchased from Immune Technology Corp. (New York, USA). Anti-HA Ab against influenza A virus (New Caledonia/20/99) (H1N1) HA (H1) and a mouse monoclonal Ab [B219M] were purchased from Abcam Inc. (Cambridge, UK). Anti-HA Ab against influenza A virus (Brisbane/10/07) (H3N2) HA (H3) and a rabbit polyclonal antibody were purchased from Sino Biological Inc. (Beijing, China). Recombinant influenza virus A (New Caledonia/20/99) (H1N1), A (Netherlands/219/03) (H7N7) and A (Hong-Kong/1073/99) (H9N2) were purchased from Prospec-Tany TechnoGene Ltd. (Rehovot, Israel). Goat anti-rabbit IgG-HRP was purchased from Santa Cruz Biotechnology (CA, USA). Tetramethylbenzidine (TMBZ) was purchased from Dojindo (Kumamoto, Japan). Clinically isolated influenza virus A/Yokohama/110/2009 (H3N2) was provided by Dr. C. Kawakami of the Yokohama City Institute of Health, Japan. Anti-Norovirus (NoV) antibody (NS-14) that is broadly reactive with the NoV genogroup II was developed and

characterized as previously described (**Kitamoto et al., 2002; Kou et al., 2015**). Norovirus-like particles (NoV-LPs) that were previously prepared in our laboratory were used for the detection of NoV-LPs.

2.2. Equipment

UV/vis absorption and fluorescence emission measurements were carried out using a filter-based multimode microplate reader (Infinite® F500; TECAN, Ltd, Männedorf, Switzerland). Transmission electron microscopy (TEM) images were obtained using a TEM (JEM-2100F; JEOL, Ltd., Tokyo, Japan) operated at 100 kV. Powder X-ray diffraction (PXRD) analysis was carried out using a RINT ULTIMA XRD (Rigaku Co., Tokyo, Japan) with a Ni filter and a Cu-K α source. Data were collected over $2\theta = 5\text{--}60^\circ$ at a scan rate of $0.01^\circ/\text{step}$ and 10 s/point . Zeta potential and dynamic light scattering (DLS) measurements were performed using a Zetasizer Nano series (Malvern Inst. Ltd., Malvern, UK). Energy dispersive spectroscopy (EDS) analysis was carried out using a scanning electron microscopy system (JEM-16036; JEOL, Ltd., Tokyo, Japan) LA integrated with JED-2300 EDS. Conjugation of the Ab to the QDs and GNP was confirmed using a plate reader from Bio-Rad (Model 680; Hercules, USA).

2.3. Synthesis of quaternary-alloyed CdSeTeS core QDs

Organometallic hot-injection synthesis of quaternary-alloyed CdSeTeS core QDs was carried out according to a previously reported method with modifications (**Adegoke et al., 2015**). Briefly, in a 3-necked flask fitted with a thermometer and a refluxing condenser, 1.3 g of CdO was stirred in a solution of 0.6 g of HDA, 2.23 mL of TOP, 50 mL of 1-octadecene and 30 mL of oleic acid under an inert atmosphere. When the temperature of

the solution reached $\sim 260^{\circ}\text{C}$, a premixed TOPSe solution containing 0.3 g of Se and 1.93 g of TOPO in 25 mL of 1-octadecene was added to the Cd-HDA-OA solution. This step initiated the nucleation and subsequent growth of CdSe QDs. Formation of the alloyed quaternary CdSeTeS QDs was accomplished by swiftly adding TOPTe solution (containing 0.48 g of Te and 1.93 g of TOPO dissolved in 25 mL of 1-octadecene) and TOPS solution (containing 0.16 g of S and 1.93 g of TOPO dissolved in 25 mL of 1-octadecene). The hydrophobic quaternary-alloyed CdSeTeS QDs were washed using methanol followed by acetone and were retained in chloroform until further use.

2.4. Surface modification of the hydrophobic CdSeTeS QDs with L-cysteine

Surface modification of the hydrophobic QDs with the L-cysteine thiol ligand was carried out via a ligand exchange reaction. A methanolic-KOH-L-cysteine solution was prepared by dissolving 3 g of KOH in 40 mL of methanol. Once the KOH pellets were completely dissolved, 2 g of L-cysteine was added to the solution and was allowed to dissolve via ultrasonication. The hydrophobic QDs in chloroform solution were added to the methanolic-KOH-L-cysteine solution, and an appropriate volume of ultrapure deionized (DI) water was added to precipitate the hydrophilic QDs from solution. The solution was stirred for several minutes and was allowed to stand overnight for complete separation of the organic phase from the water-soluble phase. The QDs were repeatedly purified using acetone and chloroform. All experiments were carried out using ultrapure DI water ($> 18 \text{ M}\Omega\cdot\text{cm}$).

2.5. Synthesis of AuNPs

AuNPs were synthesized from HAuCl_4 in HEPES buffer according to a previously reported procedure (**Rong et al., 2010**). Briefly, 1 mL of HAuCl_4 solution (20 mM) was

mixed with 4 mL of HEPES buffer and 36 mL of ultrapure DI water. The color of the solution changed to purple within 30 min of reaction time based on the slow formation of AuNPs in HEPES buffer. The AuNPs were purified by centrifugation ($6500 \times g$, 20 min) and were subsequently dissolved in 2 mL of ultrapure DI water. Thereafter, the surface of the AuNPs was capped with the L-cysteine thiol ligand by adding an appropriate amount of KOH and adjusting the pH of the solution to 11. Next, 0.2 g of L-cysteine was added, and the solution was stirred for 2 hr. L-cysteine-capped AuNPs were purified by centrifugation and were subsequently dissolved in 2 mL of ultrapure DI water.

2.6. Conjugation of antibodies to AuNPs and alloyed L-cysteine-CdSeTeS QDs

Anti-NA Ab was conjugated to L-cysteine-thiolated AuNPs using EDC/NHS covalent chemistry. Briefly, 100 μ l of 0.1 M EDC was added to 2 mL of AuNP solution to activate the carboxylate groups on the surface of the nanoparticles. The solution was stirred at ambient temperature for 30 min. Next, 100 μ l of 0.1 M NHS was added and the mixture was stirred for \sim 5 min followed by the addition of 5.1 μ g/mL of anti-NA Ab. The conjugate mixture was stirred overnight at 7°C. The anti-NA Ab-conjugated AuNPs were purified by centrifugation ($3000 \times g$, 5 min) and were subsequently dissolved in 2 mL of ultrapure DI water.

For the conjugation of anti-HA Ab to L-cysteine-capped alloyed CdSeTeS QDs, EDC/NHS conjugation chemistry was also applied. Briefly, 1 mL of 0.1 M EDC was added to 2 mL of QD solution, and the mixture was stirred at ambient temperature for 30 min. Afterward 1 mL of 0.1 M NHS was added and the mixture was stirred for \sim 5 min followed by the addition of 5.1 μ g/mL HA Ab. The conjugate mixture was allowed to react overnight at 7°C. The anti-HA-Ab-conjugated CdSeTeS-alloyed QDs were purified

via centrifugation ($3000 \times g$, 5 min) and were subsequently dissolved in 2 mL of ultrapure DI water.

2.7. Confirmation of the conjugation of Abs to the nanoparticles

The conjugation of Abs to AuNPs and QDs was confirmed using ELISA. Ab-conjugated AuNPs and QDs were added to a polystyrene 96-well plate (100 μ l) and were incubated overnight at 4°C. As a negative control, 100 μ l of BSA was added to a separate well. Next, 100 μ l of 5% skim milk solution was added and applied as a blocking agent after washing 3 times with PBST (containing 1 mL of Tween in 999 mL of PBS buffer). After blocking, the 5% skim milk was removed by washing 3 times with PBST. Anti-rabbit IgG-horseradish peroxidase was diluted to 1:4000 with 2% BSA, and 100 μ l of this solution was added to the well and was incubated at ambient temperature for 1 hr. TMB (100 μ l), a chromogenic substrate, was added to the well as a coloring reagent, and confirmation of this effect was indicated by a blue color. The reaction was stopped by adding 50 μ l of 10% H₂SO₄, which changed the color of the solution from blue to yellow (Fig. S-1, Supplementary information). The absorbance of the solution was measured using a microplate reader at 450 nm with a reference filter of 655 nm.

2.8. Immunofluorescence assay for the target virus

Ab-conjugated AuNPs and Ab-conjugated QDs were mixed in a 3:1 mixture (Fig. S-2, Supplementary information) as the probe solution. In a 96-well plate, 80 μ l of the probe solution and separate 20- μ l volumes of the target were mixed and incubated for 3 min before fluorescence measurements were acquired. The detection of influenza virus (H1N1) in the concentration range of 10–100 pg/mL was carried out in DI water and in

human serum, while the detection of clinically isolated influenza virus (H3N2) in the concentration range of 10–100 PFU/mL and NoV-LPs in the concentration range of 10–100 pg/mL was carried out in DI water. The sample solution was excited at 450 nm, and the fluorescence intensity was measured in a range of 460–700 nm. The limit of detection (LOD) was calculated by multiplying the standard deviation of blank measurements (n = 10) by 3 and dividing by the slope of the linear calibration curve. The standard deviation of the blank measurement average value (n=10) was 19.1.

2.9. Detection principle of the biosensor

LSPR-induced fluorescence transduction changes were used as the detection principle for target viruses. The surfaces of L-cysteine AuNPs and L-cysteine CdSeTeS QDs were conjugated to anti-NA and anti-HA Abs, respectively, which specifically bind to antigens of the target influenza viruses. The antigens (HA and NA) on the surface of the influenza virus bind to the anti-NA Ab-conjugated AuNPs and anti-HA Ab-conjugated QDs due to their high specificity and affinity. LSPR-induced from adjacent AuNPs is used to trigger fluorescence-enhancement changes in the QDs in a concentration-dependent manner based on interactions with the target viruses (Scheme 1). In the absence of LSPR from the AuNPs, the fluorescence of the QDs was not enhanced when interacted with the virus. The fluorescence enhancement of the QDs was triggered only upon LSPR from adjacent AuNPs.

3. Results and discussion

3.1. Characterization of alloyed L-cysteine-capped CdSeTeS QDs

The hydrodynamic particle size distribution of the QDs was determined using DLS. DLS provides three basic pieces of information by (i) probing the hydrodynamic particle size distribution of the nanocrystals in solution, (ii) evaluating the monodispersity of the nanocrystals and (iii) verifying the agglomeration state of the nanocrystals. As shown in Fig. S-3A, Supplementary information, the DLS peak of the QDs shows that they are monodisperse. The hydrodynamic particle size of the QDs was measured as 10.1 ± 2.9 nm. If the QDs were polydisperse, the size distribution would be poor, and if they were aggregated, the hydrodynamic particle size would be > 100 nm. The particle size distribution and low size value provide a direct confirmation of the monodispersity and unagglomerated state of the QDs.

The morphological properties of the QDs with respect to the particle size distribution and shape were further probed using TEM. A monodisperse particle size distribution was obtained while the particle shape was consistently spherical across the entire TEM monograph, as shown in Fig. 1A. The average particle size of the QDs was 3.8 nm and hydrodynamic size was two times bigger (Fig. S-3A, Supplementary information). Alloyed L-cysteine-capped CdSeTeS QDs were obtained via a ligand exchange reaction by exchanging the hydrophobic capping agents of OA, TOPO and HDA with L-cysteine. The optical properties of the QDs were characterized using UV/vis absorption and PL emission measurements. Band edge absorption and PL emission spectra were exhibited by the QDs, indicating that the deep trap emission was significantly suppressed. The maximum absorption of the QDs measured at the first excitonic peak occurred at 608 nm, while the PL emission maximum was found at 634 nm (Fig. 1B). The PL quantum yield (QY) of the QDs was measured to judge the quality of the QDs. We measured the PL QY of our synthesized alloyed L-cysteine-CdSeTeS QDs as 57%. This relatively high value

suggests that the surface defect states in the QDs were considerably suppressed.

Zeta potential (ZP) measurements of unconjugated and Ab-conjugated QDs were carried out to probe the degree of colloidal stability of the nanocrystals. Fig. S-3B and S-3C, Supplementary information, show ZP curves for the unconjugated and Ab-conjugated QDs, respectively. Based on the general criteria used in probing the colloidal stability of nanoparticles when applied in drug delivery systems, ZP values in the range of ± 30 mV imply that the nanoparticle is highly stable and ZP values in the range of $\pm 10-20$ mV imply that the nanoparticle is relatively stable. The ZP value obtained for the unconjugated QDs is -50.1 ± 6.9 mV, while the value obtained for the Ab-conjugated QDs is -17.1 ± 3.4 . The data imply that the unconjugated QDs exhibit high colloidal stability, while the Ab-QDs exhibit relative colloidal stability. The decreased stability of the Ab-QDs is due to the strong binding of the Ab to the QDs, which is reflected by fluorescence quenching of the latter. Further probing of the colloidal stability of Ab-QDs using ZP when measured in water and human serum as a function of pH is discussed in Fig. S-4 and Table S-1, Supplementary information.

PXRD was used to characterize the crystal nature of the QD nanocrystals. The diffraction pattern of the QDs, as shown in Fig. 2A, signifies that the QDs are crystalline and cubic in nature. The diffraction pattern exhibiting three notable peaks at planes $\{111\}$, $\{220\}$ and $\{311\}$ corresponds to the zinc-blend crystal structure. The broad nature of the peaks indicates the nanocrystallite dimension of the QDs.

A qualitative measurement of the elemental metal components of the chalcogenide QD material was obtained using EDS. Fig. 2B shows an EDS plot for the L-cysteine-CdSeTeS QDs. The elements Cd, Se, Te and S were identified as some of the semiconductor metal components of the QDs, while the elements C and O were identified

as some of the elements on the surface-capped L-cysteine ligand. The elemental composition is Cd (35.32%), Se (0%), Te (4.24%), S (7.42%), O (47.03%) and C (5.98%). Se metal displayed a 0% composition, implying that it was buried deep inside the core material, hence making X-ray identification difficult.

3.2. Characterization of AuNPs

AuNPs were prepared in HEPES buffer and were further capped with L-cysteine thiol ligand. L-cysteine was used in this work due to its stabilizing potential, its strong binding affinity and the terminal carboxylate group needed for bioconjugation. Fig. 3A shows the UV/vis absorption spectrum of the L-cysteine-capped AuNPs, where a relatively broad SPR band was observed.

The structural properties of the nanoparticles were determined using TEM, ZP and DLS measurements. TEM images of the AuNPs showed that they are quasi-spherical (Fig. 3B). The ZP of the AuNPs was investigated to probe their surface charge and colloidal stability. Fig. S-3D and S-3E, Supplementary information, show ZP curves for the AuNPs and Ab-conjugated AuNPs. A single Gaussian peak without the presence of peak splitting was obtained. The ZP values were -22.7 mV for the AuNPs and -12.1 mV for the Ab-conjugated AuNPs. These results imply that unconjugated AuNPs exhibit relative stability while a moderately stable colloidal state was exhibited by the Ab-conjugated AuNPs. Further investigation of the colloidal stability of Ab-AuNPs using ZP when measured in water and human serum as a function of pH is discussed in Fig. S-4 and Table S-1, Supplementary information.

DLS was further used to determine the hydrodynamic particle size distribution of the nanoparticles and to probe for particle agglomeration. The DLS distributions of the

AuNPs and Ab-AuNPs are shown in Fig. S-3F and S-3G, Supplementary information, respectively. A hydrodynamic particle size of 32.40 ± 12.1 nm was obtained for the unconjugated AuNPs, while for the Ab-conjugated AuNPs, a value of 49.48 ± 18.2 nm was obtained. Both the AuNPs and Ab conjugated-AuNPs had a hydrodynamic particle size < 100 nm. This finding provides direct evidence of the monodisperse particle state of the AuNPs and indicates that this morphology was not altered even after conjugation to the Abs. The increased hydrodynamic particle size of the Ab-conjugated AuNPs relative to the AuNPs is due to the binding effect of the Abs.

3.3. Detection of target viruses

Detection of the influenza virus (H1N1) was carried out in DI water and in human serum. Human serum was used as a detection medium to demonstrate the ability of the biosensor to detect influenza virus in complex biological media. Fig. 4A and B show the LSPR-induced immunofluorescence enhancement for the detection of influenza virus (H1N1) in water and in human serum, respectively. The QDs are used as a fluorophore signal generator whose sensitivity is enhanced by LSPR from adjacent AuNPs. At increasing concentrations of influenza virus, progressive enhancement of the QD fluorescence was achieved both in water and in human serum. Moreover, no notable peak shift was observed in the detection of the target H1N1 virus, providing evidence that the QDs were highly stable during the detection period. A corresponding linear calibration curve is shown in Fig. 4C. The LOD for the detection of the influenza virus (H1N1) in ultrapure DI water is 0.03 pg/mL, while the LOD in human serum is 0.4 pg/mL. A comparison of our LOD with other published values shows the improved sensitivity of our detection system (Table 1). The measurement time was ~ 5 min after the addition of

the target virus. Hence, our immunofluorescence biosensor system is much faster than RIDTS, which requires ~15 – 20 min, and RT-PCR, which requires several hours for detection.

The versatility of our biosensor was further applied for the detection of clinically isolated influenza virus (H3N2) and NoV-LPs. LSPR-induced immunofluorescence enhancement was successfully applied for the detection of the target H3N2 virus (Fig. 5A) and NoV-LPs (Fig. 5C). As the virus concentration increased, progressive increases in the fluorescence intensity of the QD fluorophore were achieved. Corresponding regression calibration curves with a linear response are shown in Fig. 5B and D. The obtained LOD for the H3N2 virus is 10 PFU/mL, and the LOD for the NoV-LPs is 0.4 pg/mL. The results show that our LSPR-induced immunofluorescence biosensor is versatile and can be applied to the detection of other target viruses.

To verify that LSPR signal from AuNPs influences the sensitivity of the biosensor, we carried out a test using Ab-QDs without LSPR for the detection of the targeted virus. As shown in Fig. S-5, Supplementary information, the fluorescence emission of the Ab-QDs after addition of the target virus was quenched, hence indicating that without LSPR signal, the target virus cannot be detected. The fluorescence enhancement signal of the QDs induced by LSPR was ~3.6 fold for H1N1, ~1.8 fold for H3N2 and ~2.5 fold for NoV-LPs.

3.4. Specificity of the nanobiosensor

The specificity of the LSPR-induced immunofluorescence biosensor for the detection of the target influenza virus (H3N2) at 10^4 PFU/mL was investigated. A 2% BSA solution, NoV-LPs, influenza viruses H7N7 and H9N2 were used as a negative control to judge the

specificity of the biosensor. The fluorescence intensity generated using the LSPR-induced immunofluorescence biosensor for the target influenza virus (H3N2) was greater than that for the negative control (Fig. 6), demonstrating the specificity of our biosensor for the target virus.

4. Conclusion

An LSPR-induced immunofluorescence nanobiosensor for influenza virus has been developed with high sensitivity, rapidity and specificity. In the biosensor, LSPR from adjacent AuNPs can trigger the fluorescence enhancement of QDs based on an antibody-antigen interaction when in direct contact with the target influenza virus. Successful detection of the influenza virus in water and in human serum was accomplished. The versatility of the biosensor was successfully applied for the detection of clinically isolated influenza virus (H3N2) and NoV-LPs.

Acknowledgements

OA thanks the Japan Society for the Promotion of Science (JSPS) for a postdoctoral fellowship (No. 26-04354). This work was supported by the Suzuken Memorial foundation, Japan, and partly by the Bilateral Joint Research Project of the Japan Society for the Promotion of Science, Japan.

Appendix A. Supplementary material

Supplementary data associated with this article can be found in the online version at:

References

- Adegoke, O., Kato, T., Park E.Y., 2016. *Biosens. Bioelectron.* 83, 483–490.
- Adegoke, O., Nyokong, T., Forbes, P.B.C. 2015. *J. Alloy. Compd.* 645, 443–449.
- Adegoke, O., Seo, M-W., Kato, T., Kawahito, S., Park E.Y., 2016. *J. Mater. Chem. B* 4, 1489–1498.
- Ahmed, S.R., Hossain, M.A., Park, J.Y., Kim, S.H., Lee, D., Suzuki, T., Lee, J., Park, E.Y., 2014. *Biosens. Bioelectron.* 58, 33–39.
- Ahmed, S.R., Hossain, M.A., Park, J.Y., Kim, S.H., Lee, D., Suzuki, T., Lee, J., Park, E.Y., 2014. *Biosens. Bioelectron.* 58, 33–39.
- Ahmed, S.R., Kim, J., Suzuki, T., Lee, J., Park, E.Y., *Biotechnol. Bioeng.* in press. doi: 10.1002/bit.25982.
- Anderson, R.E., Chan, W.C.W., 2008. *ACS Nano* 2, 1341–1352.
- Bimbo, L.M., Denisova, O.V., Mäkilä, E., Kaasalainen, M., De Brabander, J.K., Hirvonen, J., Salonen, J., Kakkola, L., Kainov, D., Santos, H.A., 2013. *7*, 6884–6893.
- Bruchez, M., Moronne, M., Gin, P., Weiss, S., Alivisatos, A.P., 1998. *Science* 281, 2013–2016.
- Campbell, C.T., Kim, G., 2007. *Biomaterials* 28, 2380–2392.
- Centres for Disease Control and Prevention (CDC). Seasonal Influenza (Flu). Guidance for Clinicians on the Use of Rapid Influenza Diagnostic Tests. Available from URL: http://www.cdc.gov/flu/professionals/diagnosis/clinician_guidance_ridt.htm
- Chan, W.C.W., Nie, S.M., 1998. *Science*, 281, 2016–2018.
- Chang, Y.F, Wang, S.F., Huang, J.C., Su, L.C., Yao, L., Li, Y.C., Wu, S.C, Chen, Y.M., Hsieh, J.P., Chou, C., 2010. *Biosens. Bioelectron.* 26, 1068-1073.
- Christman, M.C., Kedwaii, A., Xu, J., Donis, R.O., Lu, Guoqing., 2011. *Infect. Genet. Evol.* 11, 803–811.

- Eum, N.-S., Lee, S.-H., Lee, D.-R., Kwon, D.-K., Shin, J.-K., Kim, J.-H., Kang, S.-W., 2003. *Sensor. Actuat. B-Chem.* 96, 446–450.
- Garcia-Cañas, V., Lorbetskie, B., Bertrand, D., Cyr, T.D., Girard, M., 2007. *Anal. Chem.* 79, 3164–3172.
- Girarda, M.P., Tam, J.S., Assossou, O.M., Kieny M.P., 2010. *Vaccine* 28, 4895–4902.
- Grabowska, I., Malecka, K., Stachyra, A., Góra-Sochacka, A., Sirko, A., Zagórski-Ostoja, W., Radecka, H., Radecki, J., 2013. *Anal. Chem.* 85, 101067–10173.
- Hay, A., Gregory, V., Douglas, A., Lin, Y., 2001. *Philos. Trans. R. Soc. Lond. B Biol. Sci.* 356, 1861–1870.
- Jarocka, U., Sawicka, R., Góra-Sochacka, A., Sirko, A., Zagórski-Ostoja, W., Radecki, J., Radecka, H., 2014. *Sensors.* 14, 15714–15728.
- Jeong, E.-J., Jeong, Y.S., Park, K., Yi, S.Y., Ahn, J., Chunga, S.J., Kim, M., Chung, B.H., 2008. *J. Biotechnol.* 135, 16–21.
- Kitamoto, N., Tanaka, T., Natori, K., Takeda, N., Nakata, S., Jiang, X., Estes, M.K., 2002. *J. Clin. Microbiol.* 40, 2459–2465.
- Kou, B., Crawford, S.E., Ajami, N.J., Czakó, R., Neill, F.H., Tanaka, T., Kitamoto, N., Palzkill, T.G., Estes, M.K. Atmar, R.L., 2011. *Clin. Vaccine Immunol.* 22, 160–167.
- Landry, M.L., 2011. *Curr. Opin. Pediatr.* 23, 91–97.
- Lee, G.C., Jeon, E.S., Kim, W.S., Le, D.T., Yoo, J.H., Chong, C.K., 2010. *Viol J.* doi: 10.1186/1743-422X-7-244.
- Lee, J., Ahmed, S.R., Oh, S., Kim, J., Suzuki, T., Parmar, K., Park, S.S., Lee, J., Park, E.Y., 2015. *Biosens. Bioelectron.* 64,311–317.
- Leung, C-H., Tseng, H-K., Wang, W-S., Chiang, H-T, Wu, A.Y.-J., Liu, C-P., 2014. *J. Microbiol. Immunol.* 47, 518–525.

- Özyer, Ş., Ünlü, S., Çelen, Ş., Uzunlar,Ö., Saygan, S., Su, F.A., Besli, M., Danışman, Nuri., Mollamahmutoğlu, Leyla., 2011, *Taiwan. J. Obstet. Gyne.* 50, 312–317.
- Patskovsky, S., Jacquemart, R., Meunier, M., De Crescenzo, G., Kabashin, A.V., 2008. *Sensor. Actuat. B-Chem.* 133, 628–631.
- Pianciola, L., González, G., Mazzeo, M., Navello, M., Quidel, N., Bulgheroni, M.F., 2010. *Rev. Panam. Salud. Publica.* 27, 452–454.
- Rong, C., Jiliang, W., Hui, L., Gang, C., Zhong, Lu., Chi-Ming, C.H.E. 2010. *Rare Metals.* 29, 180–186.
- Tian, J., Zhao, H., Liu, M., Chen, Y., Quan, X., 2012. *Anal. Chim. Acta* 723, 83–87.
- Treanor, J.J., 2005. Influenza virus. In: G. L. Mandell, J. E. Bennett, R. Dolin, editors. *Principles and Practice of Infectious Disease.* 2nd ed. Philadelphia, PA: Churchill Livingstone; p.2060.
- Yeom, S-H., Han, M-E., Kang, B-H., Kim, K-J., Yuan, H., Eum, N-S., Kang, S-W., 2013. *Sensor. Actuat. B-Chem.* 177, 376–383.

Figure legends

Scheme 1. Schematic representation of the detection principle for the influenza virus using the LSPR-induced fluorescence nanobiosensor.

Fig. 1. Morphology and photophysical properties of L-cysteine CdSeTeS core QDs. (A) TEM image of L-cysteine CdSeTeS QDs and (B) UV/vis absorption (dotted line) and fluorescence emission spectra (solid line) of L-cysteine CdSeTeS core QDs.

Fig. 2. Structural properties of L-cysteine CdSeTeS core QDs. (A) Powder XRD patterns of L-cysteine CdSeTeS core QDs and (B) EDS spectrum of L-cysteine CdSeTeS QDs.

Fig. 3. Morphology and physical properties of AuNPs. (A) UV/vis absorption spectrum of AuNPs and (B) TEM image of AuNPs and ZP distributions of AuNPs.

Fig. 4. PL emission spectra showing the detection of the influenza virus (H1N1) using the LSPR-induced immunofluorescence biosensor in (A) ultrapure DI water and (B) in human serum. (C) Corresponding PL calibration curve for detection of the influenza virus in DI water and in human serum. Errors bars in (C) denote standard deviation of 3 replicate measurements.

Fig. 5. PL emission spectra and corresponding PL calibration curves of sample viruses. (A) PL emission spectra showing the detection of clinically isolated influenza virus (H3N2) using the LSPR-induced immunofluorescence biosensor. (B) Corresponding PL calibration curve of the H3N2 influenza. (C) PL emission spectra showing the detection of NoV-LPs using the LSPR-induced immunofluorescence biosensor. (D) Corresponding PL calibration of NoV-LPs. Errors bars in (B) and (D) denote standard deviation of 3

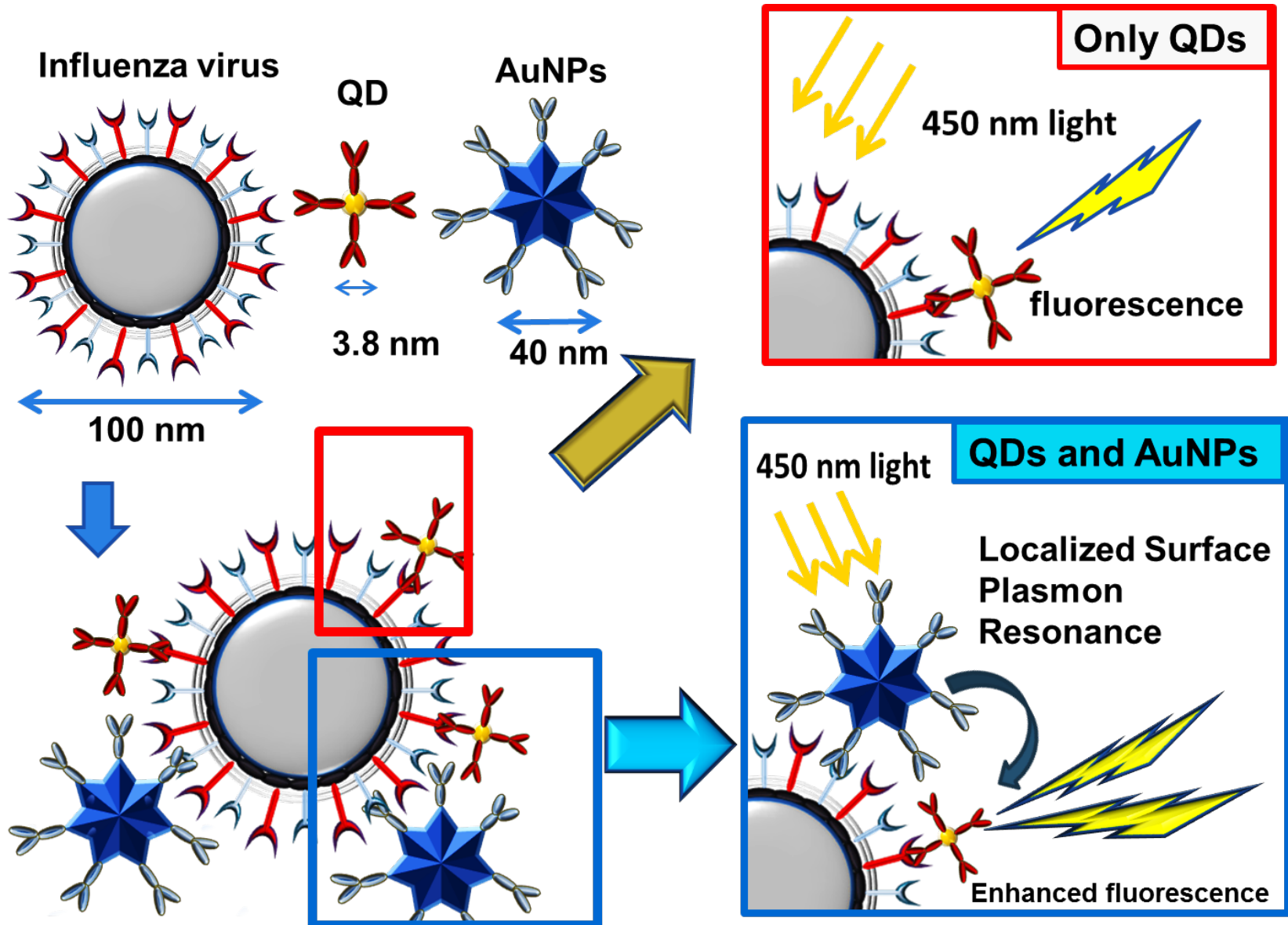
replicate measurements.

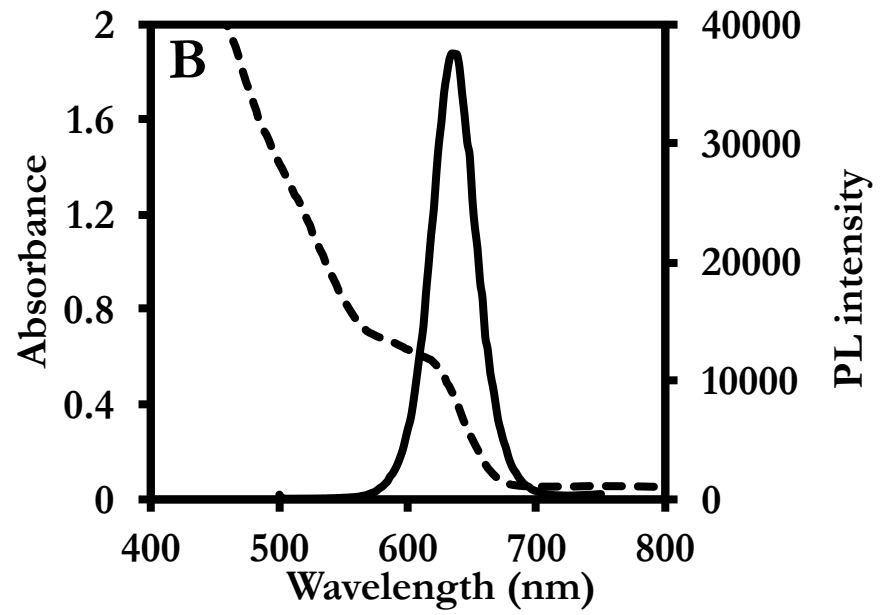
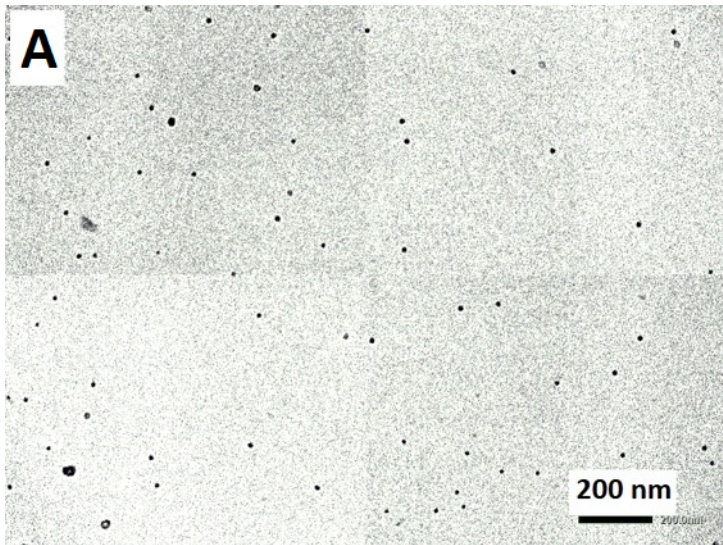
Fig. 6. Specificity of the LSPR-induced immunofluorescence biosensor. Anti-NA Ab-conjugated AuNPs and anti-HA (H3N2) Ab-conjugated CdSeTeS core QDs were used to evaluate the specificity of the LSPR-induced immunofluorescence biosensor. The used analyte was pure water, 2% BSA solution, 30 $\mu\text{g}/\text{mL}$ of NoV-LPs and 10^4 PFU/mL of the influenza virus (H3N2). Errors bars denote standard deviation of 3 replicate measurements.

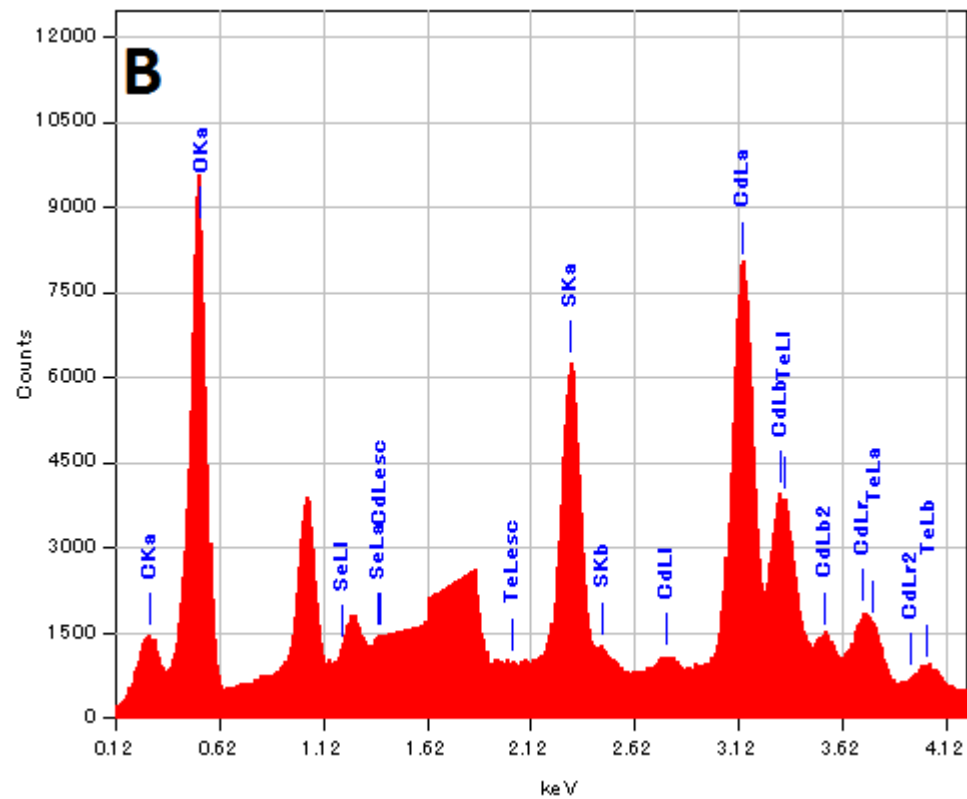
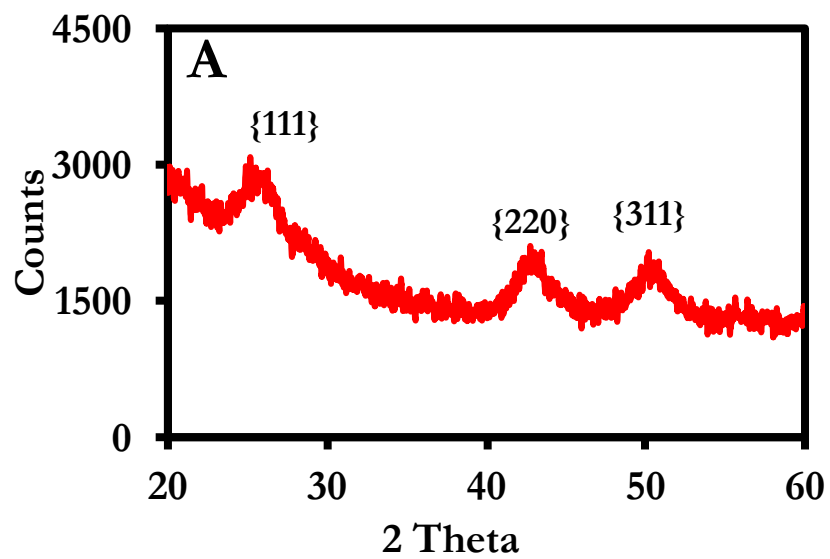
Table 1.

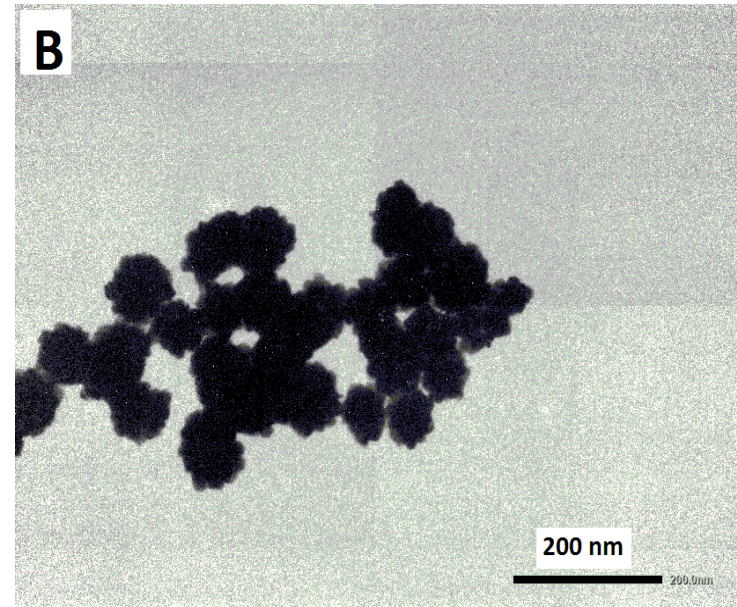
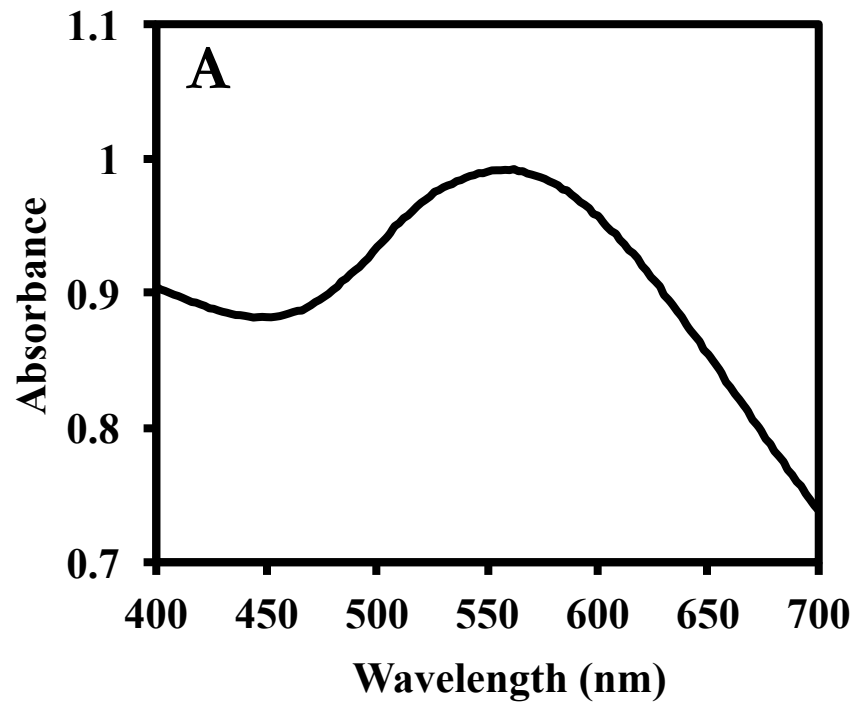
Comparison of the detection limit of the proposed LSPR-induced fluorescence immunobiosensor

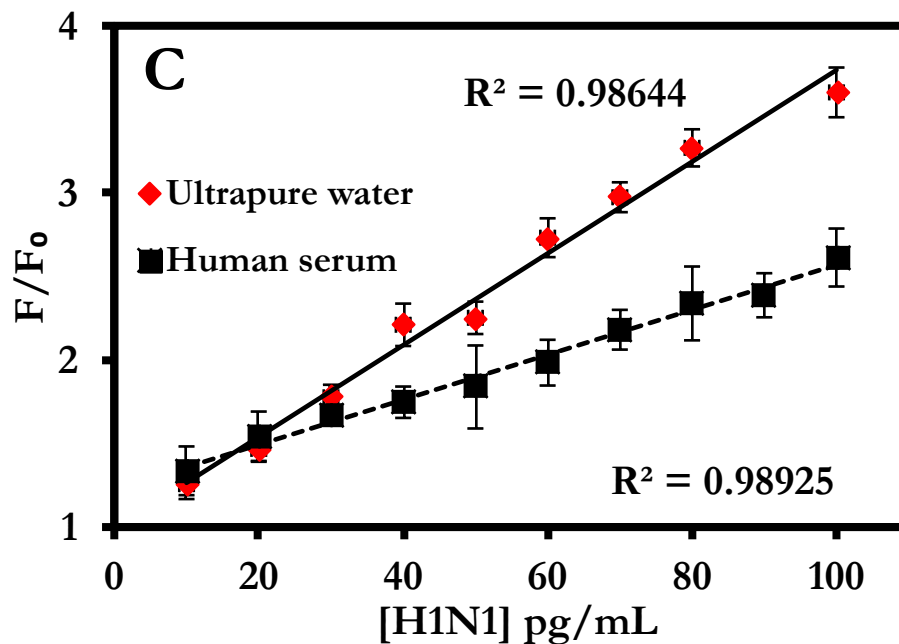
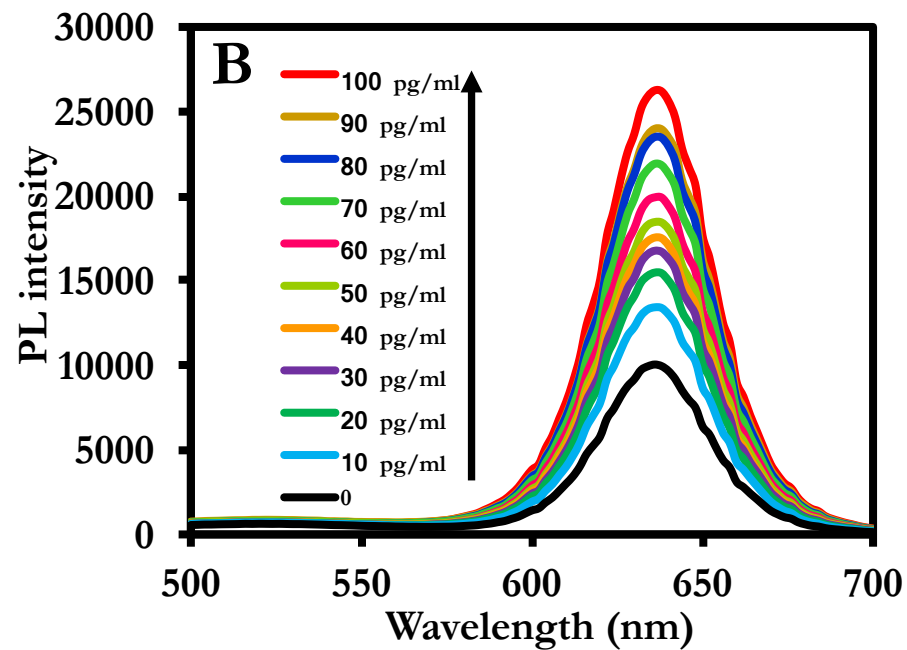
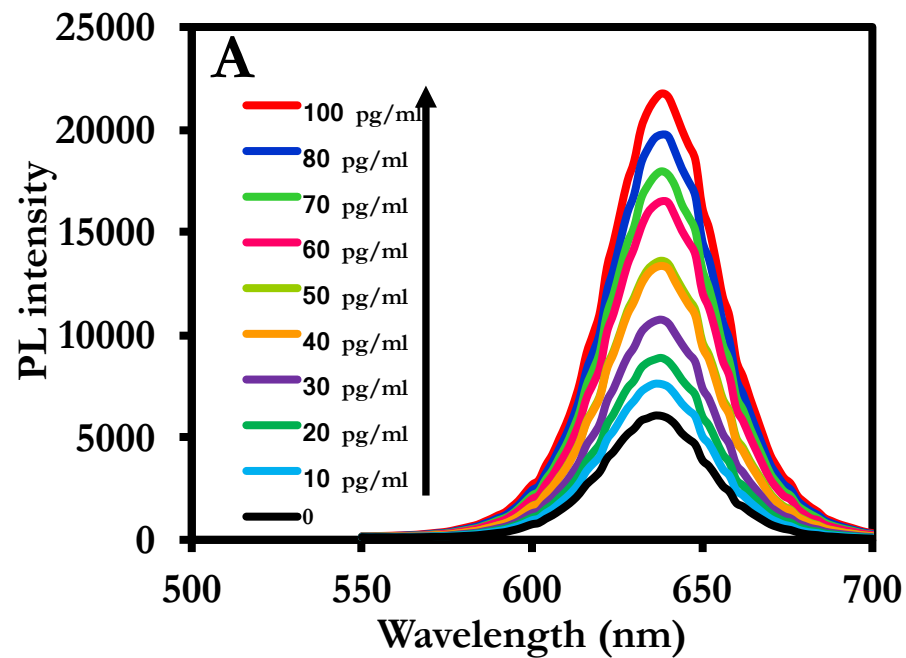
Detection technique	H1N1 strain	Signal type	LOD	Reference
LSPR-induced immunofluorescence	A/New Caledonia/20/99	Fluorescence enhancement	0.03 pg/mL	This work
Metal enhanced fluorescence	A/New Caledonia/20/99	Fluorescence enhancement	1 ng/ml	Ahmed et al. (2014)
Peroxidase mimic	A/New Caledonia/20/99	Colorimetric	10 pg/mL	Ahmed et al. (2016)
LSPR fiber-optic	A/Vietnam/1203/2004	Fluorescence enhancement	13.9 pg/mL	Chang et al. (2010)
2D-HPLC method	A/New Caledonia/20/99	HPLC-fluorescence	105 ng/mL	Garcia-Cañas et al. (2007)
Electrochemical immunosensor	A/Poland/08/2006	Electrodes	2.2 pg/ml	Jarocka et al. (2014)
Immunochromatography assay	A/California/12/2009	Colorimetric	73 ± 3.65 ng/ml	Lee et al. (2010)

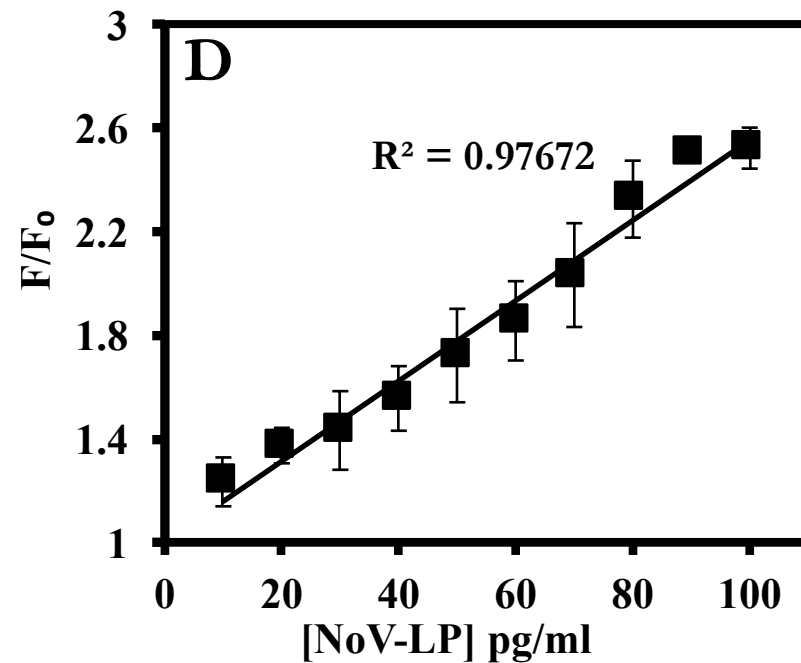
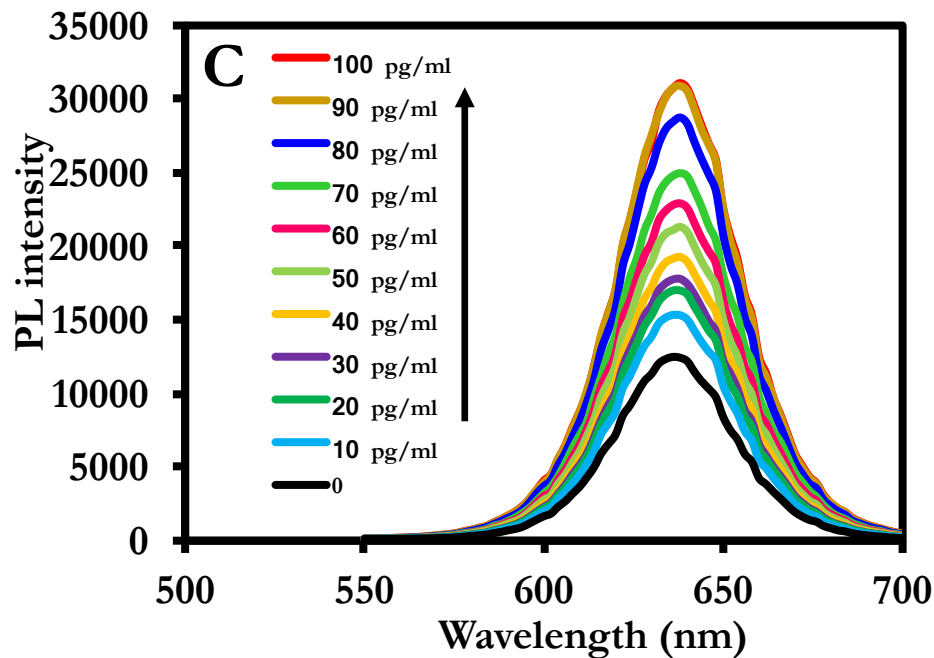
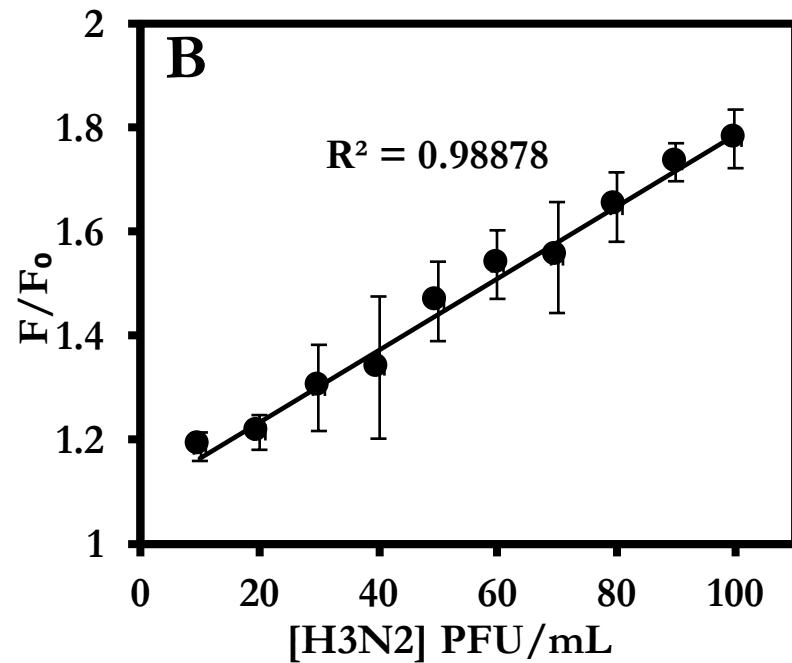
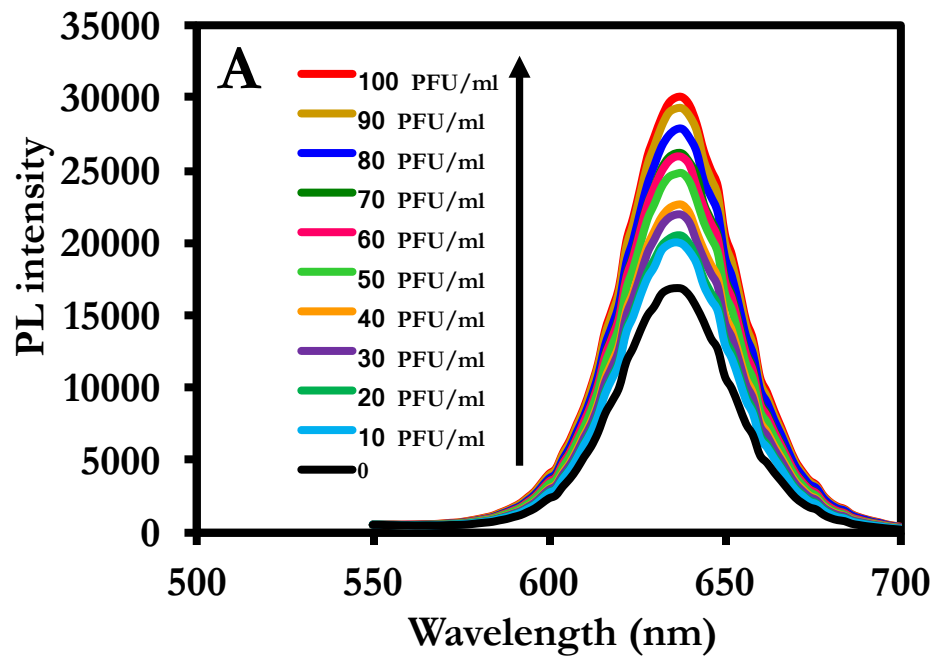


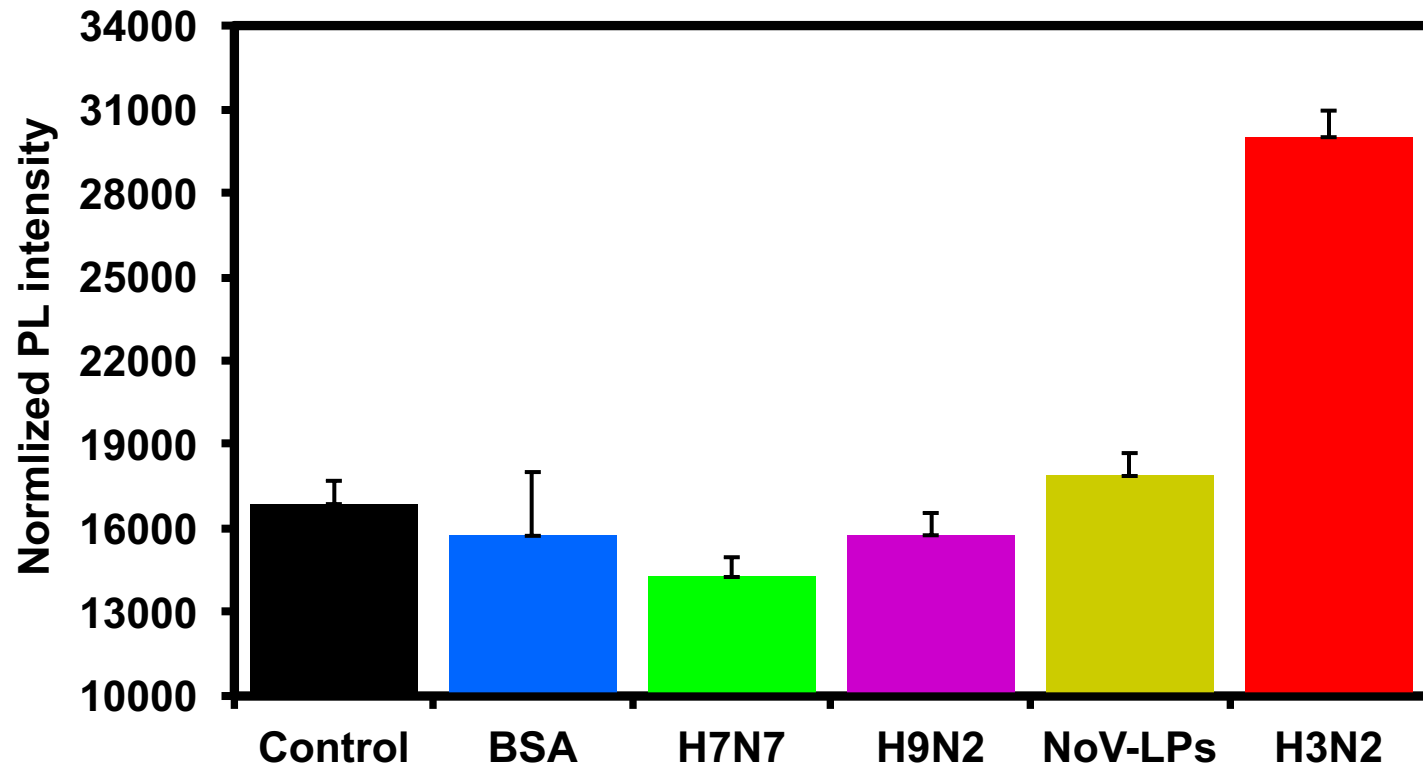












Supplementary Information

Versatility of a localized surface plasmon resonance-based gold nanoparticle-alloyed quantum dot nanobiosensor for immunofluorescence detection of viruses

Kenshin Takemura^a, Oluwasesan Adegoke^b, Naoto Takahashi^a, Tatsuya Kato^{b,c}, Tian-Cheng Li^d, Noritoshi Kitamoto^e, Tomoyuki Tanaka^f, Tetsuro Suzuki^g, and Enoch Y. Park^{b,c,1}

^a *Laboratory of Biotechnology, Department of Agriculture, Graduate School of Integrated Science and Technology, Shizuoka University, 836 Ohya, Suruga-ku, Shizuoka 422-8529, Japan*

^b *Laboratory of Biotechnology, Research Institute of Green Science and Technology, Shizuoka University, 836 Ohya, Suruga-ku, Shizuoka 422-8529, Japan*

^c *College of Agriculture, Academic Institute, Shizuoka University, 836 Ohya, Suruga-ku, Shizuoka 422-8529, Japan*

^d *Department of Virology II, National Institute of Infectious Diseases, Gakuen 4-7-1, Musashi-Murayama, Tokyo 208-0011, Japan*

^e *School of Human Science and Environment, University of Hyogo, 1-1-12 Shinzaike-Honcho, Himeji, Hyogo 670-0092, Japan*

^f *Hidaka General Hospital, Gobo, Wakayama 644-0002, Japan*

^g *Department of Infectious Diseases, Hamamatsu University School of Medicine, 1-20-1 Higashi-ku, Handa-yama, Hamamatsu 431-3192, Japan*

E-mail:

kenpi901@yahoo.co.jp (KT)

adegoke.sesan@mailbox.co.za (OA)

pakkun0449@yahoo.co.jp (TN)

kato.tatsuya@shizuoka.ac.jp (TK)

litc@nih.go.jp (TCL)

kitamoto@shse.u-hyogo.ac.jp (NK)

moqui-tom@maia.eonet.ne.jp (TT)

tesuzuki@hama-med.ac.jp (TS)

park.enoch@shizuoka.ac.jp (EYP)

¹ Correspondence to: Research Institute of Green Science and Technology, Shizuoka University, 836 Ohya Suruga-ku, Shizuoka, 422-8529, Japan. Tel. & fax: +81 54 238 4887. E-mail address: park.enoch@shizuoka.ac.jp (EYP)

ELISA assessment

The binding effect of the Ab to the QDs and AuNPs was confirmed using ELISA. As shown in Fig. S-1, the absorbance of the Ab-QDs and Ab-AuNP at 450 nm was stronger than the absorbance obtained using QD-BSA and AuNP-BSA as negative control. The results confirms that the Ab was successfully bonded to the QDs and AuNP.

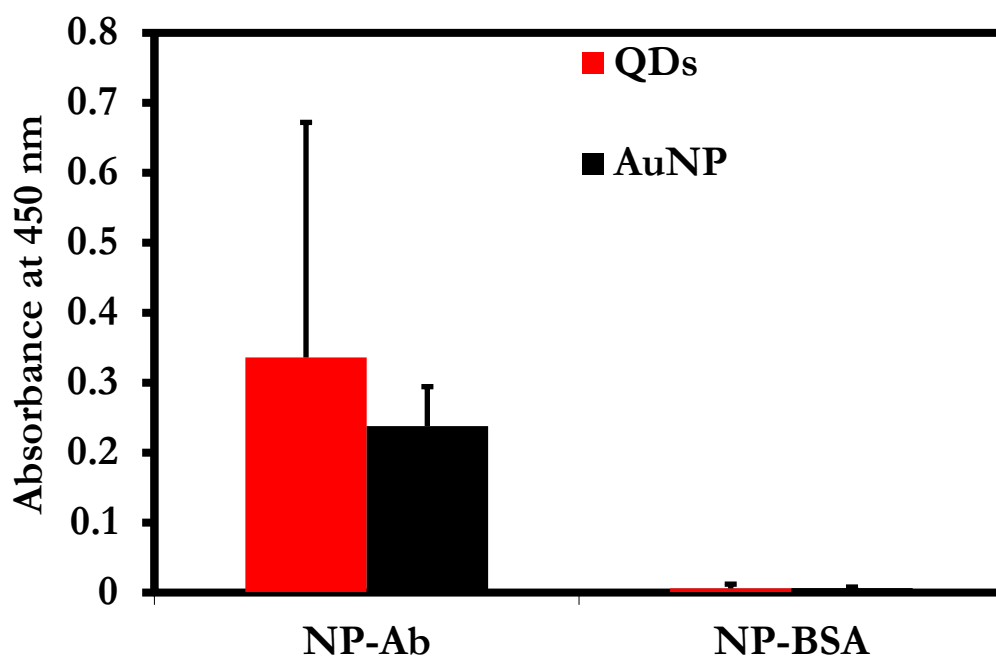


Fig. S-1. ELISA data confirming the binding of the antibodies to AuNP and the QDs.

Optimization of the detection solution

The stoichiometric ratio of the QDs and AuNPs which can generate optimum PL enhancement signal was investigated. The following ratios were prepared: AuNPs:QDs (2:1), AuNPs:QDs (1:1), AuNPs:QDs (1:2), AuNPs:QDs (1:3). As shown in Fig. S-2, optimum PL enhancement signal for the target detection of 100 ng/ml of influenza virus H1N1 was obtained at AuNPs:QDs (1:3). Hence, AuNPs:QDs (1:3) was chosen as the stoichiometric ratio.

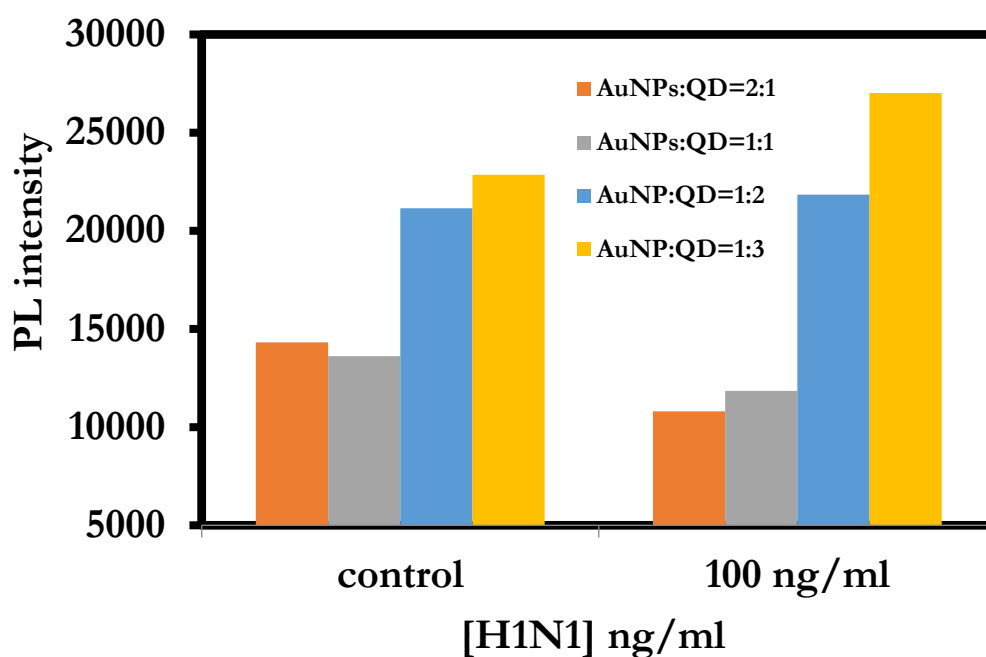


Fig. S-2. Determination of the stoichiometric ratio between AuNPs and QDs for the target detection of influenza virus.

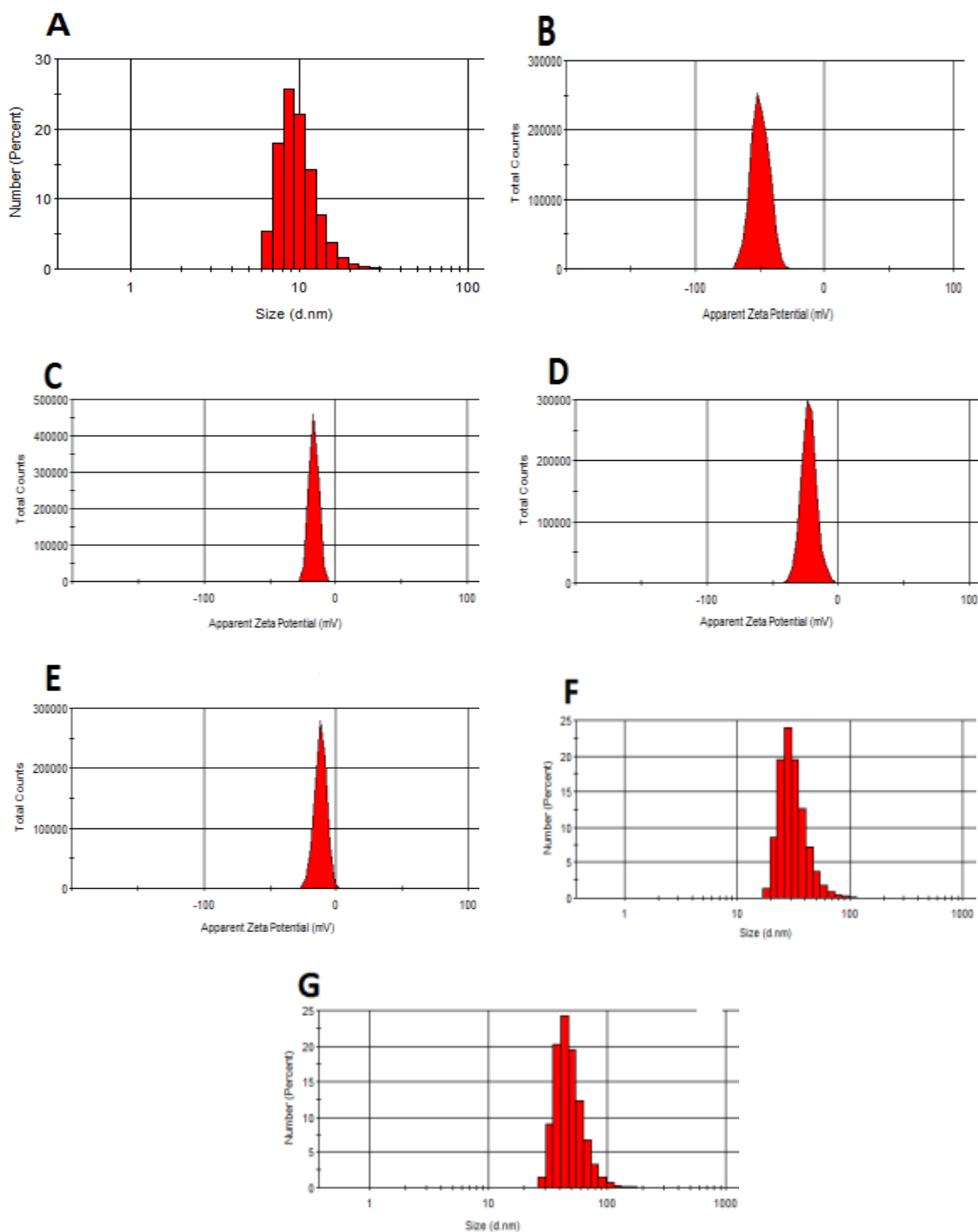


Fig. S-3. (A) DLS hydrodynamic size of *L*-cysteine CdSeTeS core QDs, (B) ZP distributions for the unconjugated QDs, (C) Ab-conjugated QDs, ZP distributions of (D) AuNPs and (E) anti-NA Ab-conjugated AuNPs, DLS hydrodynamic size distributions of (F) AuNPs and (G) anti-NA Ab-conjugated AuNPs.

Effects of pH on the ZP of Ab-conjugated QDs and Ab-conjugated AuNPs

Further analysis of the ZP of Ab-conjugated QDs and Ab-conjugated AuNPs as a function of pH in water and in human serum was studied. For the ZP measurements in human serum, dilution with water was 1000:1 (water:human serum). Fig. S-4A and S-4B shows the plots of the ZP charge as a function of pH for the Ab-QDs and Ab-AuNPs while Table S-1 displays the corresponding ZP charge. The first direct observation shows the absence of ZP data at pH 11 which is due to agglomeration and loss of colloidal stability of the conjugates. As shown in Fig. S-4A, for Ab-AuNPs, the ZP charge increased as the pH increased in both water and human serum, thus indicating that the ZP charge was dependent on the pH. Using the colloidal stability guideline: highly unstable (± 0 –10 mV), relatively stable (± 10 –20 mV), moderately stable (± 20 –30 mV) and highly stable (± 30 mV), the ZP charge in Table S-1 for Ab-AuNPs, shows that it ranged from highly unstable (pH 3, water) to highly stable (pH 9, human serum). For Ab-QDs, the ZP charge increased as the pH increased when measured in human serum but decreased as the pH increased from 3 – 7 and afterward increased at pH 9 when measured in water. Results shows that the colloidal stability ranged from highly unstable (pH 3, human serum) to highly stable (pH 9, water and human serum).

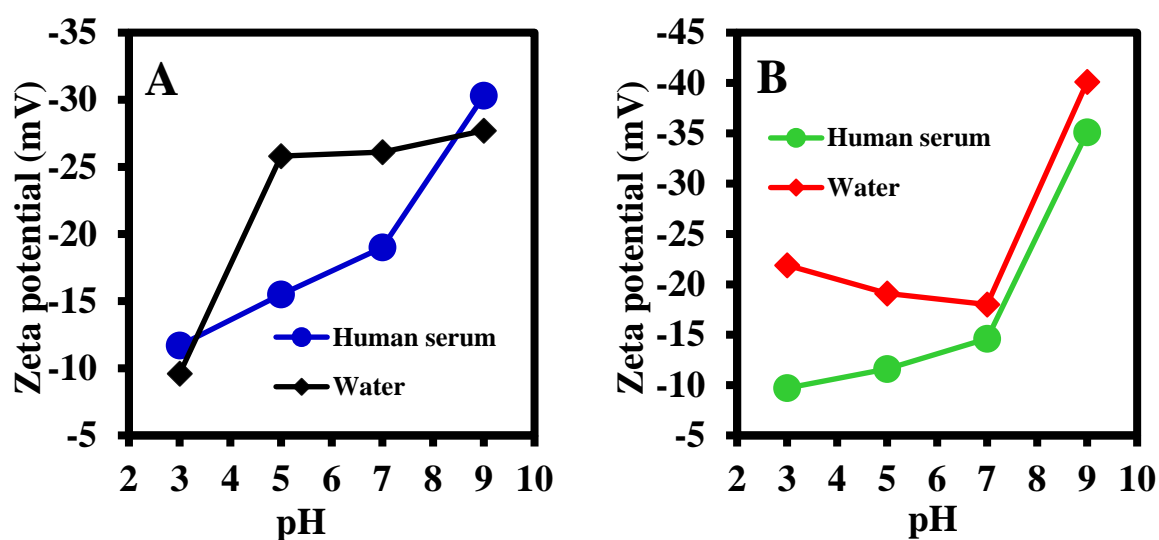


Fig. S-4. Plots of the ZP as a function of pH in water and human serum for Ab-AuNPs (A) and Ab-QDs (B).

Table S-1. Effects of pH on the ZP of Ab-conjugated QDs and Ab-conjugated AuNPs in human serum.

pH	Ab-QDs ^a [mV]	Ab-AuNPs ^a [mV]	Ab-QDs ^b [mV]	Ab-AuNPs ^b [mV]
3	-21.9±4.8	-9.6±7.2	-9.7±3.2	-11.7±6.6
5	-19.1±3.5	-25.8±8.8	-11.6±3.7	-15.5±5.9
7	-18.0±4.4	-26.1±8.9	-14.6±4.6	-19.0±5.9
9	-40.1±3.9	-27.7±11.9	-35.1±13.9	-30.3±9.6
11	-	-	-	-

^aWater; ^bHuman serum

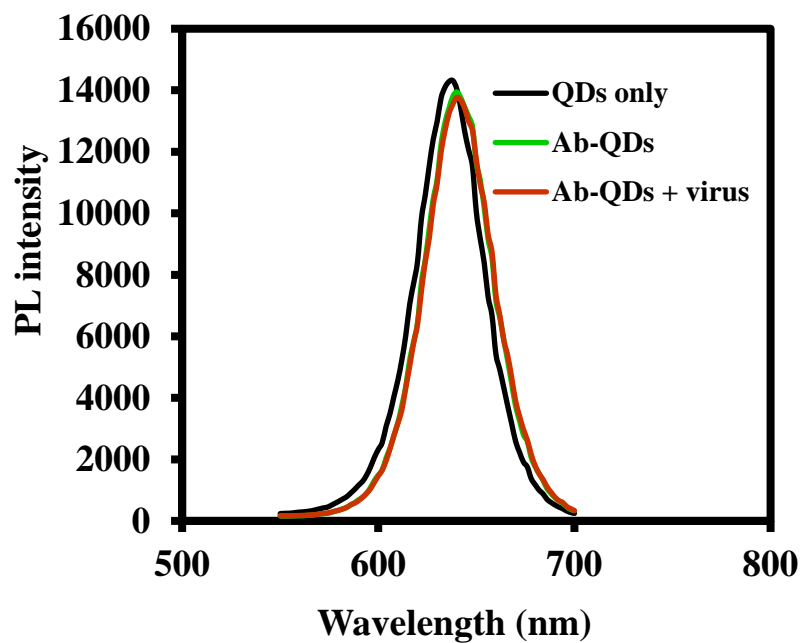


Fig. S-5. The emission spectra of the QDs only, Ab-QDs and Ab-QDs with virus target (no LSPR-induced signal).